Nanoscale

Accepted Manuscript

This article can be cited before page numbers have been issued, to do this please use: K. Voitchovsky, *Nanoscale*, 2016, DOI: 10.1039/C6NR05879E.

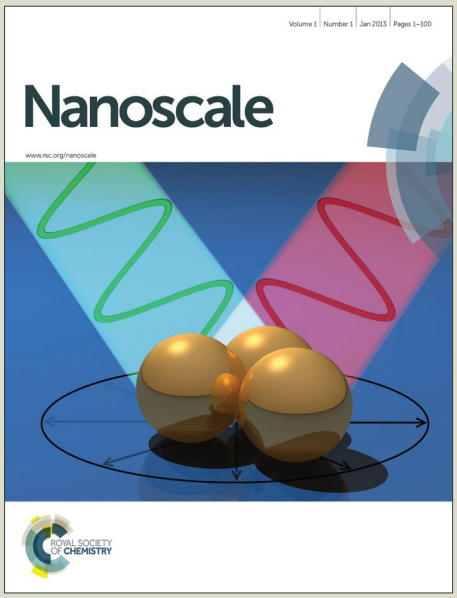

ROYAL SOCIETY OF CHEMISTRY

www.rsc.org/nanoscale

View Article Online
DOI: 10.1039/C6NR05879E

Nanoscale

ARTICLE

Effect of temperature on the viscoelastic properties of nano-confined liquid mixtures

Received 00th January 20xx,
Accepted 00th January 20xx

DOI: 10.1039/x0xx00000x

www.rsc.org/

Kislon Voïtchovsky[a]

The behaviour of fluids confined in nanoscale gaps plays a central role in molecular science and nanofluidics, with applications ranging from biological function to multiscale printing, osmosis and filtration, lab-on-chip technology and friction reduction. Here atomic force microscopy is used to shear five different mixtures of hexadecane and squalane confined between the tip apex and atomically flat graphite. The shearing amplitudes are typically < 2 nm, hence reflecting highly localised information at the interface. The evolution of each mixture's viscoelastic properties is studied as a function of temperature, between 20 °C and 100 °C. The results, complemented by sub-nanometre resolution images of the interface, show that spatial organisation of the liquid molecules at the surface of graphite largely dominates the measurements. Squalane presents a higher affinity for the surface and forms a robust self-assembled layer in all mixtures. This results in a step-like change of the viscous and elastic response of the confined liquid as the confining pressure increases. In contrast, measurements in pure hexadecane show a continuous and linear increase in the apparent viscosity with pressure at all temperatures. This is interpreted as a more fragile interfacial layer and images show that it can be completely removed at high temperatures. Depending on the mixture composition, measurements can be strongly location-dependent which suggests molecular clustering and nanoscale phase separation at the interface.

Introduction

Nano-confined liquids play an important role in countless systems, ranging from transport in protein channels and pores[1,2] to nanofluidics-based technologies[3,4] such as 3D printing[5,6] water purification[7], single molecule detectors[8,9], lab-on-chip technology[10] and the control of dynamical contacts between macroscopic solids in motion[11-14]. In most real-life systems, the confined liquid is not pure, but composed of a mixture of molecules[15]. The liquid is typically sheared with respect to a solid wall, either by force flow in nano-channels[2,8,10,16] or by confinement between moving solids[11,17]. The behaviour of the sheared liquid has a large impact on the efficiency of the process considered. This behaviour can generally not be inferred from measurements on the bulk liquid. Given the small scale of a nano-confined system, the specific molecular details, the geometry and structure of the confining solids, the presence of impurities as well as the measurement itself can all considerably influence the results[12,18-20].

Several studies have reported confinement-induced phase transitions[21,22] and increases of several orders of magnitudes in the 'effective' viscosity of the liquids under shear[23-27]. Despite ongoing debates regarding the behaviour of confined water[18,24-26,28], it is generally accepted that nano-confined liquids tend to exhibit structural and viscoelastic properties dramatically different from those of their bulk counterpart[29]. The interface between the liquid and the confining surfaces often dominate the nano-confined liquid's behaviour[11], in particular for systems where the liquid exhibits some affinity for the surface[27]. At the macroscopic scale, when a liquid meets a solid, the resulting interface can be quantified through so-called contact-angle measurements[30,31] that determine the wetting properties of the liquid – that is, its affinity for the surface. At the molecular level, a wetting liquid indicates strong interactions between the liquids molecules and the solid[32,33]. These interactions as well as reduced configurational entropy result in the interfacial liquid molecules being usually more ordered and less mobile than in bulk liquid[34,35]. A 'wetting' interfacial liquid often exhibit molecular layering parallel to the solid's surface, but this structure decays rapidly into the bulk liquid, usually over a few molecular diameters[19,36]. In the case of nano-confined liquids, two solid-liquid interfaces are brought in close proximity and the thickness of the resulting liquid film becomes comparable to that of the interfaces. As a result, both confined interfaces may significantly influence the behaviour of the confined liquid molecules which tend to become globally more ordered than bulk liquid, often forming layers[27,37-43]. Intuitively, this is can be understood by combining the properties of both interfaces with a further loss of entropy for the liquid molecules. This confers the confined properties close to that of a solid or a glass, reflected by an important increase in the apparent

[a] Physics Department, Durham University, Durham DH1 3LE, UK.
Email: kislon.voitchovsky@durham.ac.uk

Electronic Supplementary Information (ESI) available: supplementary methods and figures S1-S5. See DOI: 10.1039/x0xx00000x

viscosity and elasticity[24,26,27,39,44]. Although intuitive, this understanding is far from absolute since molecular details such as orientation, structural arrangement or ability to slip at the surface of the solid can play a significant role[12,20,45]. Computer simulations can provide invaluable insights into such details, in particular for dynamic systems[29,46].

Experimentally, nano-confined liquids are typically studied with the surface force apparatus[11,21,22,28,39,43,47-52] (SFA) or with atomic force microscopy (AFM)[25-27,40,42,53-66]. The SFA offers a close to perfect confinement geometry between atomically flat surfaces, an absolute measurement of the distances between the surfaces down to sub-angstrom resolution and it can apply shear forces to the system. In contrast, the AFM confines liquids between a poorly controlled nanoscale tip (typically 5-10 nm radius) and a flat surface, but it allows for considerably higher applied pressures, imaging of the interface with sub-nanometre spatial resolution[32,33,58,67], and a high flexibility with the choice of confining materials.

Here AFM is used to compare five different mixtures of hexadecane and squalane sheared between a silicon oxide tip and an atomically flat highly ordered pyrolytic graphite (HOPG) surface as a function of temperature and confining force. The setup used for the experiment is inspired by that developed in the lab of E. Riedo[26,68], and allows for measurement of both the viscous and elastic response of the confined liquid as a function of the tip-sample distance. Significantly, the shear amplitude is relatively small (< 2 nm) which allows for a high spatial resolution of the shear measurement. This is important in liquid mixtures or on uneven surfaces where differences in liquid behaviour can occur between different locations. The results confirm that the organisation of the liquid molecules at the surface of graphite largely dominates the measurements. When present in the liquid, squalane molecules form a robust interfacial monolayer with the molecules oriented upright on the surface. The layer, which remains intact even at 100 °C, induces a step-like increase of the viscous and elastic response of the confined liquid as the confining pressure increases. In contrast, measurements in pure hexadecane show a continuous and linear increase in the apparent viscosity with pressure at all temperatures, with little elastic response. Depending on the liquid mixture, measurements can be strongly location-dependent which suggests molecular clustering and nanoscale phase separation at the interface with HOPG.

The results illustrate the importance of molecular details for determining the viscoelastic properties of confined liquids. This is particularly true for liquid mixtures where a single component can completely dominate the observed behaviour, or nanoscale phase separation can induce strong local effects.

Experimental

Sample preparation and experimental conditions

Hexadecane (Hd) and squalane (Sq) were purchased from Sigma-Aldrich (Dorset, UK). The stated purity of both liquids was >99% and they were used without further purification. The fusion and vaporisation temperatures of the pure liquids (T_f and T_v respectively) are T_f = 18 °C and T_v = 287 °C for Hd, and are T_f = -38 °C and T_v = 176 °C for Sq. Five different solutions were prepared from binary Hd:Sq mixtures: 1:0 (pure Hd), 3:1, 1:1, 1:3, and 0:1 (pure Sq). All the mixtures appeared completely soluble in bulk at all temperatures. Measurements in the pure liquids served as reference. Each mixture was sonicated at 30 °C until optically homogenous and kept at room temperature.

The substrate, highly ordered pyrolytic graphite (HOPG) (SPI supplies, West Chester, PA) was glued to a steal disc with epoxy resin (Araldite, Basel, Switzerland), ensuring direct contact between the graphite and the metal. This is necessary to achieve good thermal conduction throughout the substrate and favour accurate temperature settings during the measurement. The HOPG was freshly cleaved before each set of measurement using adhesive tape and immediately covered with the solution studied. For each of the 5 liquids probed (Hd, Hd3:1Sq, Hd1:1Sq, Hd1:3Sq, and Sq), the study was conducted at 20 °C, 30 °C, 40 °C, 50 °C, 60 °C, 70 °C, 80 °C, 90 °C, 100 °C (always ±0.1°C), and repeated at least 3 times with a new tip.

Temperature control. In order to allow precise and reproducible temperature-controlled measurement, a heating/cooling system with precision better than ±0.1°C was used. The system is integrated in the AFM and accessible through the AFM control software. The temperature is measured in the metallic sample support. The use of a conducting HOPG substrate glued to a metal disc enables good thermal conductivity through the sample. After any change in temperature, the system was allowed to settle so as to ensure minimal drift and thermal equilibrium before measurements were conducted. The heating/cooling rates imposed by the temperature regulation loop were monitored against time, and it was estimated that thermal equilibrium was reached when the rates became constant within ±1%. This strategy allowed sub-nanometre resolution imaging at all temperatures.

AFM measurements

All the measurements were carried out on a commercial Cypher ES AFM system (Oxford Instruments, Santa Barbara, CA) equipped with temperature control. Two types of measurements were conducted complementarily: shearing and imaging. All measurements were conducted with ArrowUHF-AuD cantilevers (Nanoworld, Neuchâtel, Switzerland, nominal vertical spring constant of $k_v \sim 2$ N/m). Each cantilever was calibrated (k_v) using its thermal spectrum[69]. Torsional calibration of the cantilever's inverse optical lever sensitivity and spring constant k_t are more demanding. Given the triangular shape of the cantilever, there is currently no simple calibration method available. The calibration was therefore conducted only on a few cantilevers so as to determine an order of magnitude. The procedure used was adapted from established techniques[70,71] and is described in detail in supplementary information (see Fig. S1). It yielded a value of ~200 N/m for k_t. This is however an estimate resting on important simplifications (see Supplementary

View Article Online
DOI: 10.1039/C6NR05879E

Methods) and the results hence display only the shear amplitude, not force. The measurements were conducted with both the cantilever and the HOPG substrate fully immersed into the liquid (Fig. 1a). Each set of measurement was repeated at three times with a different cantilever/tip and in no particular order so as to ensure statistical reliability of the results.

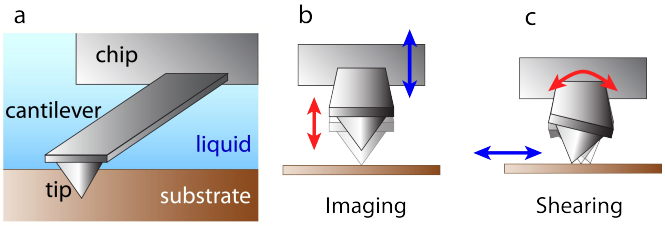

Fig. 1 Cartoon representation of the AFM tip and cantilever at the surface of HOPG in liquid (a). When used for imaging (b), the cantilever is externally driven at its resonance frequency (blue arrow) resulting in a net vertical oscillation of the tip (red arrow). The tip oscillation is damped as the tip interacts with the interfacial liquid near the substrate. In shear experiment (c), the substrate is oscillated laterally (blue arrow). As the tip approaches the interface, liquid-mediated tip-substrate coupling can induce torsion of the cantilever (red arrow).

High-resolution imaging. When used for imaging, the AFM was operated in amplitude modulation (AM-AFM). In AM the cantilever is oscillated vertically at a frequency close to its natural resonance. A detection system records the oscillation amplitude A and phase φ of tip in the liquid. Given the relatively high viscosity and poor thermal conductivity of the fluid, the cantilever oscillation was driven acoustically. Away from the substrate, the tip oscillates in the bulk liquid with a constant amplitude A_i (free amplitude). The phase $\varphi_i = \pm 90°$ due to viscous damping of the cantilever motion in the liquid. As the tip is brought closer to the sample, the oscillation amplitude decreases due to tip-interface interactions so that $A < A_i$ (Fig. 1b). Imaging is achieved by raster scanning the surface while maintaining the amplitude to a set value A_s (setpoint amplitude) using a feedback loop that constantly readjust the average tip-sample distance. The phase lag φ_s between the driving signal and tip oscillation is allowed to vary freely and changes depending on the local tip-sample interactions. Topographic images are obtained from the vertical corrections applied to average tip-sample distance when keeping the setpoint amplitude constant. In this study, the typical setpoint amplitudes were $A_s <$ 1 nm and setpoint/free amplitude ratio were kept relatively high ($A_s/A_i \sim$ 0.7-0.9) so as to ensure imaging conditions preserving the sample. Under these conditions, the images are mainly of the liquid structured at the interface rather than the solid substrate underneath[32,33,67,72]. The phase, recorded for each position scanned, carries information about local changes in the viscoelastic properties of the interfacial liquid layers imaged and is hence sensitive to variations in the structural arrangement of the molecules images, often with sub-nanometre resolution[32,67,73-75].

Shear-force spectroscopy. The shearing measurements were conducted using custom-made adaptations of the AFM software that re-assigned a lock-in amplifier to the torsional signal of the cantilever. During a typical measurement, the immersed HOPG substrate was oscillated laterally at a frequency of 1.1 kHz and an amplitude of about 2 nm using the AFM scanner (Fig. 1c). This frequency was below the natural resonance of the scanner (around 2 kHz). Standard force-distance curves were then acquired while simultaneously recording the tip vertical deflection and lateral torsion due to liquid-mediated coupling with the substrate. The amplitude A_t and phase φ_t of the torsion signal were extracted using one of the lock-in amplifiers of the AFM. The magnitude of the shearing force F_s is directly proportional to A_t. For small torsion amplitudes (as is here) we can write $F_s = k_t A_t$ with k_t the torsional spring constant of the cantilever. The phase lag φ_t between the lateral oscillation of the sample and that of the cantilever torsion caries information about the nature of the tip-substrate coupling through the sheared liquid: if $\varphi_t = 90°$, the coupling is purely viscous while for $\varphi_t = 0°$ the cantilever is perfectly coupled to the substrate and the sheared liquid behaves purely elastically (Fig. 1c). Shearing measurements are 'blind' in the sense that they are done over a particular location of the sample without knowledge of the local topography. Complementary high-resolution imaging conducted at the location immediately before or after shearing measurements allows this problem to be overcome. It also ensures that a suitable location is selected for the measurement, for example away from surface defects and singularities which might artificially affect the results. More than 100 shear curves were acquired over five randomly selected locations for each liquid, at each temperature probed. The results were analysed using routines programmed in Igor Pro (Wavemetrics, Lake Oswego, OR). The curves were aligned and averaged for pure liquids. In mixtures, it was common to observe different behaviour depending on the measuring location. In such case, the curves were sorted in sub-groups of similar behaviour.

It is worth noting that the experimental approach used here allows for rapid switching between imaging and shearing measurements without requiring making any change or adjustment to the system, therefore ensuring that both modes probe the same region of the sample.

Results and discussion

Results are presented sequentially for each liquid, starting from the pure liquids which serve as references for interpreting results in the mixtures.

Pure squalane

An example of a single shear curve acquired in Sq is presented in Fig. 2. The vertical deflection of the cantilever is recorded simultaneously to the shear amplitude and phase, and provides a direct measurement of the confining force applied by the tip. The shear amplitude, initially close to zero, increases in a step-like fashion as the tip approaches the surface. This indicates that the confined liquid is organised in cohesive layers at the interface with HOPG. These steps do not

follow a progressive behaviour, suggesting that the layering exists even in the absence of the confining tip. Past these initial steps, the shear amplitude tends to increase more regularly with the applied force. The shear phase is often more sensitive than the amplitude, as visible in Fig. 2. The shearing, initially only viscous in bulk liquid ($\varphi_t = 90°$) becomes viscoelastic when the liquid is confined. The phase is not defined if the shear amplitude is zero, far away from the surface. This is visible here is the large fluctuations visible for $z > 10$ nm. Interestingly, after an initial step increase, the phase remains constant with increasing confining force, indicating a steady shearing regime.

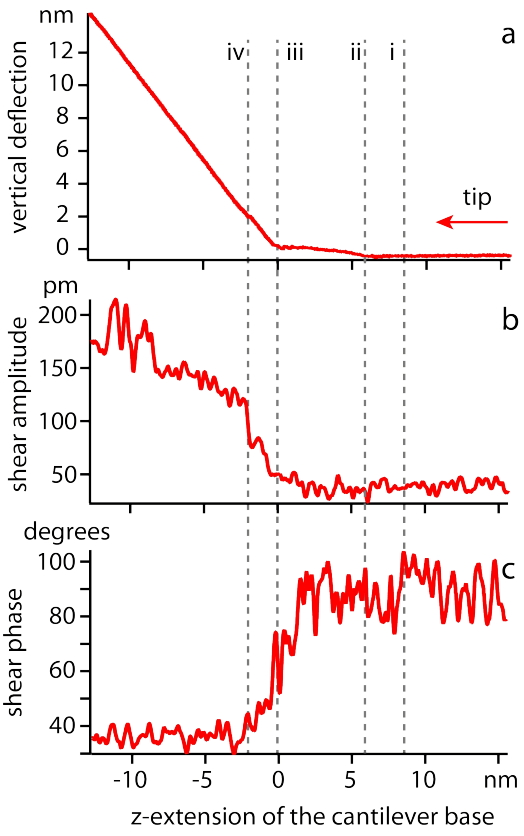

Fig 2 Example set of curves acquired during a single shear measurement in Sq at 40 °C. The vertical deflection (a), the shear amplitude (b) and the shear phase (c) are recorded simultaneously as the tip approaches the substrate. The horizontal axis indicates the extension of the base of the cantilever towards the surface. Several events can be distinguished as the tip nears the surface (from the right). Around 8 nm (i), a sudden jump in phase suggests that the tip starts interacting with the surface, but without significant change in amplitude. Around 6nm (ii), the cantilever starts deflecting vertically. This is however 'soft' with the deflection reaching a plateau and changes in amplitude and phase only starting from around 2.5 nm. At 0 nm (iii), a hard contact is established (deflection), defining arbitrarily the zero on the horizontal axis. This coincides with a jump in both phase and amplitude. As the tip-applied pressure increases (iv), a sudden jump in all channels indicates the rupture of a molecular layer confined between the tip and the sample.

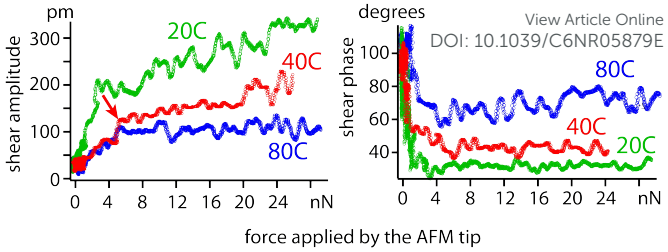

Fig 3 Representation of the shear amplitude and phase in Sq as a function of the confining force for different temperatures. The curves in red are the same as presented in Fig. 2. The main step in amplitude (labelled iv in Fig. 2) is highlighted with an arrow. The shear amplitude is still sizeable at 80 °C with in all cases an initial rapid amplitude increase in steps followed by a more progressive increase with the applied force. The phase also exhibits a characteristic step-decrease at contact (0 nN) followed by a plateau. The value of the plateau evolves with temperature from viscoelastic at 20 °C to purely viscous at 80 °C. (A purely elastic response would yield $\varphi_t = 0°$ and a purely viscous behaviour $\varphi_t = 0°$). The evolution of amplitude and phase with temperature is monotonic in Sq (see supplementary Fig. S2).

The data presented in Fig. 2 can be combined so as to place the emphasis on the region where the tip is coupled with the sample. This is done by plotting the shear amplitude and phase as a function of the cantilever vertical deflection, with the latter converted in the confining force (Fig. 3).

This presentation of the data has two advantages: first it allows for an estimate of the confining pressure between the tip and the HOPG surface. Considering a typical tip radius of 10-20 nm, the confinement area varies is about 10-100 nm^2, yielding in increase in pressure in the order of 10-100 MPa per nanoNewton applied. Second, it condenses the entire region of the curve with no force applied to a single point, therefore placing the emphasis on the relevant part of the data. Fig. 3 also shows representative shear amplitude and phases at 20 °C and 80 °C for comparison. The average behaviour of shear curves for every temperature probed is available in supplementary information (Fig. S2)

In Fig. 3, a coherent and continuous evolution can be seen in both amplitude and phase as the temperature increases. The data shows more variability past 60 °C. As the temperature increases, the shearing amplitude (and hence shear force) progressively decreases. The evolution of the shear phase with temperature indicates that the sheared Sq layer changes from viscoelastic at 20 °C to mostly viscous beyond 80°C. However, sizeable shear amplitudes are observed at all temperatures, indicating the existence of a stable and cohesive Sq molecular layer on the surface of HOPG. This is also consistent with previous results probing OMCTS/Sq mixtures at the interface with HOPG and reporting a substantial layering of the liquid[37].

The effect of temperature on the Sq-HOPG interface can be visualized directly in high-resolution images of the interfaces (Fig. 4). Initially, a thick layer is covering the surface of HOPG (20°C) with occasional defect following regular lines, indicative of a crystalline molecular packing of Sq. As the temperature increases, the thick layer leaves behind a disordered mesh of gel-like filaments, suggesting a superficial 'melting' of the top Sq layer exposed to the bulk liquid. Further temperature increase to 40°C makes the superficial Sq layer completely disappear, revealing an ordered row structure underneath.

View Article Online
DOI: 10.1039/C6NR05870E

The spacing between adjacent rows is ~4.5nm, probably due to Sq molecules lying flat on the surface. Occasional holes or cracks in the structure (not shown) indicate that the rows are formed on top of a thicker Sq layer and not directly on the HOPG substrate. At 70 °C the row structure disappears, revealing a hexagonal lattice with ~8.3 nm periodicity underneath. The presence of the hexagonal lattice suggests that the Sq molecules are not arranged parallel to the surface, but rather perpendicularly in a self-assembled monolayer. In this interpretation, the apparent periodicity results from a mismatch between the HOPG lattice and that of the hexagonally packed Sq monolayer, hence creating a hexagonal Moiré pattern. The phenomenon has previously been observed in similar systems[76,77], but usually with the self-assembled molecules lying flat on the HOPG surface. Here, given the periodicity of the HOPG lattice (2.46 Å), the intermolecular spacing of the Sq layer must be ~3.5 Å to explain the observed Moiré.

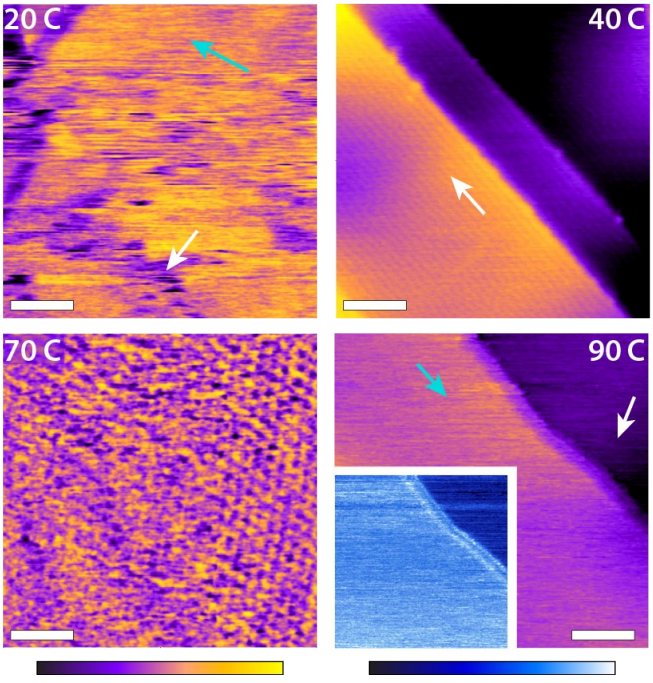

Fig 4 AFM images of Sq at the interface with HOPG at different temperatures. At 20 °C a thick layer (cyan arrow) is present and progressively 'melts' as the temperature increases (white arrow). At 40 °C, a relatively fragile row structure appears (aligned with the white arrow) underneath the 'melted' top layer. The row spacing is about 4.5 nm. At 70 °C, a hexagonal lattice (about 8.3nm periodicity) appears beneath the rows. The lattice can be explained by a monolayer of Sq self-assembled directly on the HOPG surface. The hexagonal pattern is a Moiré induced by a mismatch between the periodicities of the HOPG lattice (2.46 Å) and that of the self-assembled Sq layer (~3.5 Å). The layer remains stable up to 90 °C where different types of molecular assemblies coexist in domains: the cyan arrow point to a lattice region and the white arrow to another less ordered region. The imaging phase over the same area (inset) exhibits a clear contrast, indicating that the two regions have different molecular assemblies. All topographic images are shown in the black-purple-yellow colour scale and the phase image is shown in blue scale. The scale bars are 60 nm (20 °C), 40 nm (40 °C), 40 nm (70 °C), and 40 nm (90 °C). The colour scales represent a total height variation of 7 nm (20 °C), 2 nm (40 °C), 0.1 nm (70 °C), and 2 nm (90 °C), and a phase variation of 4° (90 °C).

This suggests strong layer cohesion due to inter-molecular van der Waals interactions, possibly strengthened by lateral interlocking of the Sq side-chains. Even past 90 °C, the lattice is still present with different types of domains that can be distinguished from local variations in the imaging phase φ_s (Fig. 4).

Throughout all experiments conducted in liquids that contained Sq, the tip was never able to reach the HOPG surface. The fact that a viscous behaviour was observed at 90 °C despite the tip not reaching the HOPG surface indicates that the behaviour of the last Sq layer was never probed; the shearing tip was probably sliding over it. This is in stark contrast with results obtained in pure Hd.

Pure hexadecane

The shear experiments conducted in pure Hd indicate a consistent and gradual decrease of the effective viscosity of the confined liquid with temperature. Figure 5 presents amplitude and phase curves as a function of the applied tip force taken at 20 °C, 40 °C and 80 °C. The complete set of average evolution for each temperature probed is available in supplementary information (Fig. S3). Increases in the confining pressure result in an almost linear increase of the shear amplitude, except at 20 °C where an initial step around 4nN, is visible. It can be explained by the tip interacting with the multiple layers formed by Hd on HOPG at room temperature[78-80]. The measured shear amplitudes become vanishingly small at higher temperatures rendering the phase considerably noisier. The phase shows little dependence on temperature, a trend confirmed for all temperatures (see supplementary Fig. S3). This is characteristic of Hd and reflects a largely viscous behaviour of the confined liquid, with little evolution as a function of the applied pressure or temperature.

The evolution of the Hd shear curves with increasing temperature is progressive, with a steady decrease of the shearing amplitude and no significant change in the phase (see Fig. S3). Unlike for Sq, the average behaviour of Hd is homogenous across the whole interface. Occasionally, substantial variations from the average behaviour were seen for individual curves at lower temperatures, suggesting some molecular organisation of the sheared liquid. These events were not common and disappeared almost entirely at higher temperatures.

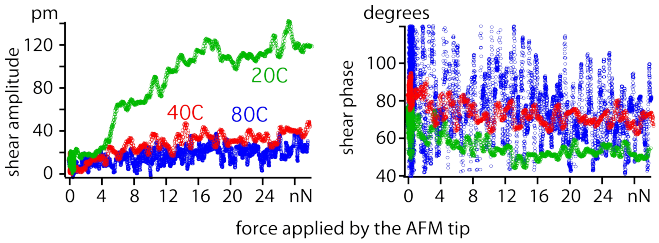

Fig 5 Representative shear amplitude and phase curves acquired in pure Hd at the surface of HOPG at 20 °C (green), 40 °C (red) and 80 °C (blue). Past 40 °C, the shear amplitude become so small that the phase is hardly detectable, resulting in noisy readings. The phase is however consistently centred around $\varphi_t = 90°$ (except at 20 °C) indicating a purely viscous behaviour (see also Fig. S3).

DOI: 10.1039/C6NR05879E

High-resolution images (Fig. 6) indicate a relatively high mobility of the Hd molecules at the interface consistent with the shear observations. At 20 °C, Hd molecules form a regular array of epitaxially-induced rows on the surface, often spanning several layers on top of each other. The distance between adjacent rows is ~2.4 nm but occasionally wider row structures are visible near surface singularities (atomic steps, layer edges). The Hd layering at room temperature and lateral organisation in rows when in contact with HOPG is a well-documented phenomenon[78,79] further confirmed here. At 50 °C, most of the row structure has 'melted' in the sense that it is less clear and more disordered with only a single layer partially visible.

At 70 °C no more structure is visible; only a uniform disordered interfacial layer with hints of temporary epitaxial effects. Finally, past 90 °C, the scanning AFM tip can fully remove the Hd molecules from the surface, revealing the underlying HOPG lattice. This occurs despite the very gentle imaging conditions (compared to shearing experiments) indicating a high mobility of the interfacial Hd molecules.

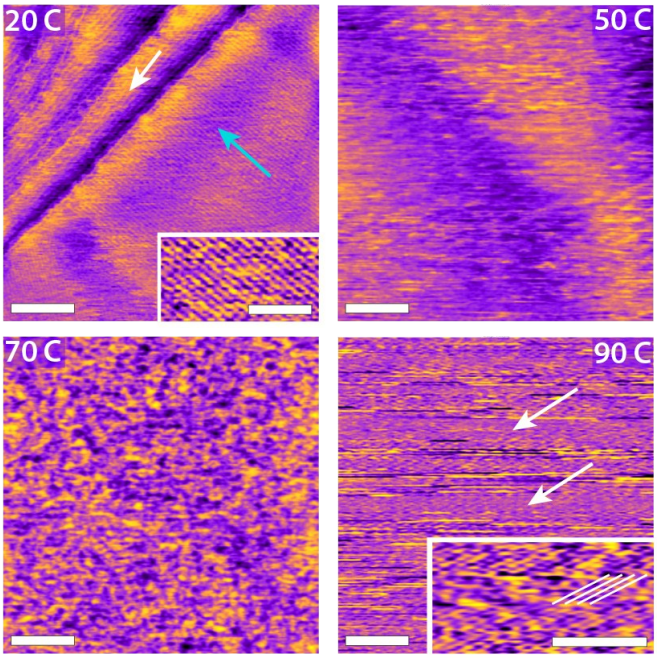

Fig 6 The interface between HOPG and Hd imaged at different temperatures. At 20 °C clear rows are visible on the surface, building up on several levels. The blue arrow indicates the direction of ~2.4 nm spaced rows. The white arrow shows wider rows occasionally observed on small regions of the surface. The inset is a magnification over a part of the image highlighted by the blue arrow. At 50 °C, the rows are visible mostly on a single level (directly on the HOPG) and are easily disrupted by the scanning AFM tip. At 70 °C, a homogenous and disordered molecular layer is visible, but there are hints of epitaxial effects. At 90°C the underlying HOPG lattice is occasionally visible as lines with ~0.25 nm spacing (along the white arrows) indicating that all the Hd can be fully removed by the scanning tip. The image is however noisy due to the Hd molecules occasionally left under the tip. The inset is a magnification over a region of the image and some HOPG atomic rows are highlighted. The colour scale is as in Fig. 4. The scale bars are 40 nm (20 °C), 20 nm (20 °C inset), 10 nm (50 °C), 10 nm (70 °C), and 2 nm (90 °C and inset). The colour scales represent a total height variation of 0.8 nm (20 °C), 0.6 nm (50 °C), 0.1 nm (70 °C), and 0.8 nm (90 °C).

Squalane:Hexadecane 3:1 mixture

Results acquired in the liquid mixtures present a much higher variability than in pure liquids, likely due to occasional nanoscale phase separation at the interface and molecular clustering within the sheared liquid. This is not so surprising given the strikingly different behaviour of Hd and Sq both in bulk and under shear[81], but it makes it difficult to present and meaningful average picture. This 'molecular segregation', confirmed by high-resolution imaging, often allows interpretation of the results as combination of Hd and Sq results. Shear force curves were more reproducible in Sq3:1Hd than in other mixtures, in particular below 60 °C where most of the variability between probed locations is usually observed (See Fig. S4 and S5). As the confining pressure increases, an initial sharp step in shear amplitude is followed by a plateau showing little change. Past 60 °C two main types of curves were observed depending on the location probed (Fig. S4), eventually converging to a single type of curves past 80 °C – 90 °C (Fig. 7).

Images in acquired in Sq3:1Hd did not reveal any particular structure such as rows or lattice. A cohesive layer is however present at all times on the surface. Different types of domain similar to those observed in pure Sq are already visible at 20°C with a clear contrast in the phase image (Fig. 8).

The behaviour of the shear force curves in Sq3:1Hd is more reproducible than in other mixtures and close to that observed in pure Sq suggesting that the Hd can be seen mainly as a small perturbation in the Sq-dominated interface. Interestingly, no ordered structure could be imaged but a molecular layer was present for all temperatures at the interface.

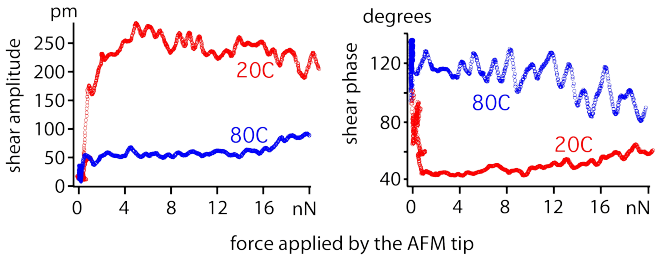

Fig 7 Selected curves representing shear amplitude and phase as a function of the applied tip force at 20 °C and 80 °C in Sq3:1Hd. The shear amplitude exhibits a step-like increase at all temperature, but with a markedly lower magnitude at higher temperature. The phase curves also exhibit the step-decrease at contact (0nN), characteristic of measurements in pure Sq (see Figs. 5 and S2). The two phase curves present a ~90° offset at 0nN, but they tend to converge towards a same value of $\varphi_t = 90°$ with increasing force. This behaviour is qualitatively reminiscent of pure Sq, but with convergence towards a completely viscous shearing.

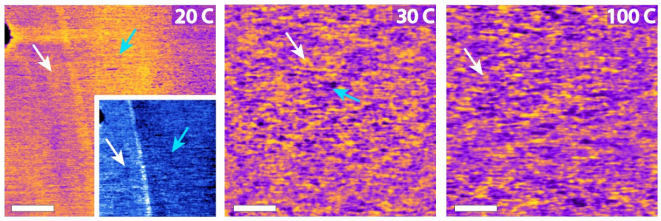

Fig 8 AFM images of HOPG in Sq3:1Hd at different temperatures. At 20°C a smooth layer is visible in topography (main frame) with occasional holes (upper left). Different molecular organisations coexist in organised domains within the layer as in pure Sq (blue and white arrow), confirmed in the phase image (inset). Little evolution is seen with temperature, with molecular islands (white arrow) or grooves (blue arrow) visible at 30°C and similarly at 100°C. The colour scale is as in Fig. 4. The scale bars are 40 nm (20 °C), 10 nm (30 °C), and 10 nm (100 °C). The colour scales represent a total height variation of 0.5 nm (20 °C), 0.16 nm (30 °C), and 0.2 nm (100 °C), and a phase variation of 4° (20 °C).

Squalane:Hexadecane 1:1 mixture

The shear forces curves in Sq1:1Hd show more variability between different locations than all other liquids and mixtures studied (see also supplementary Fig. S5). At 20°C a typical amplitude curve shows an initial step followed by a regular increase in amplitude (Fig. 9) reminiscent of observations in pure Sq (Fig. 4). As the temperature increase, the pressure applied by the tip affects mostly the shear phase with little changes in amplitude, apart for an initial step around 0 nN (seen at 80 °C in Fig. 9). The strong dependence of the shear curves on location was observed in each set of data (with new cantilevers) suggesting a wide range of different molecular organisations at the interface rather than experimental errors. This is confirmed by the fact that the shear curves were reproducible with different cantilevers in pure liquids. The phase showed and inversion of its evolution with applied force between low and higher temperatures (Fig. 9). This behaviour was also reproduced.

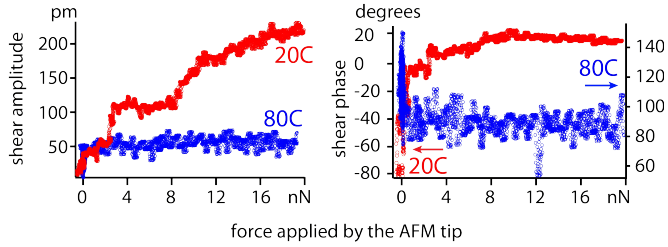

Fig 9 Selected curves representing shear amplitude and phase as a function of the applied tip force at 20 °C and 80 °C in Sq1:1Hd. The shear amplitude exhibits an evolution similar to in pure Sq at 20 °C but only a step-like increase at 80°C with limited reproducibility. The phase curves always exhibit the step-change at contact (0 nN), characteristic of measurements in pure Sq (Figs. 3 and S2). The shape of the phase curves at 20 °C and 80 °C are inverted from each other, with no obvious explanation. The inversion occurs progressively with temperature, confirming it results from temperature-induced change of molecular behaviour at the interface. If we accept that the behaviour of the sheared liquid at 20 °C is mostly elastic, then the evolution with temperature is consistent with the liquid becoming almost completely viscous past 80 °C.

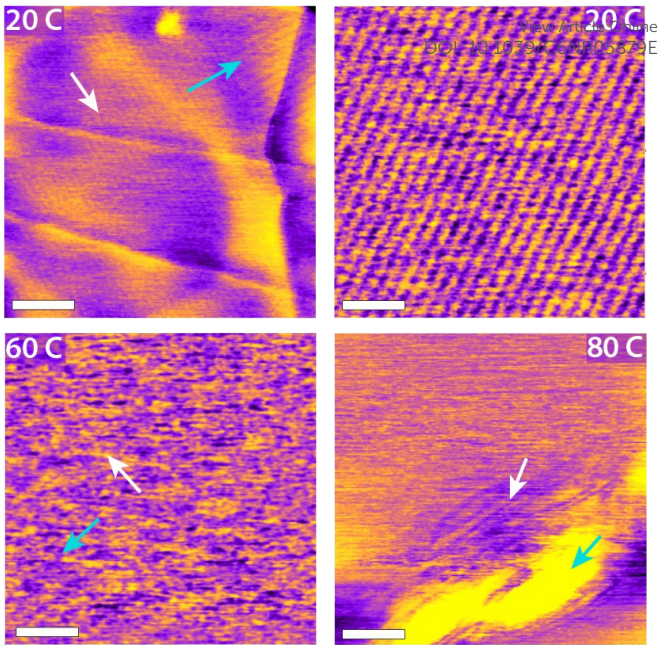

Fig 10 High-resolution AFM images of HOPG in Hd1:1Sq at different temperatures. At 20 °C rows with various spacing and orientations appear with occasional aggregates (white protrusion at the top). Hd-like rows exhibit a spacing of ~2.2 nm (white arrow) while wider rows present a ~11.5 nm spacing (blue arrow). The rows are relatively stable up to 40°C. At 60°C molecular islands (white arrow) and grooves (cyan arrows) are visible with hints of epitaxial effects (parallel to the arrows). At 80 °C large aggregates are visible (blue arrow) surrounded by stable rows/longitudinal grooves in the molecular layer (white arrow). The colour scale is as in Fig. 4. The scale bars are 100 nm (20 °C, left), 10 nm (20 °C, right), 4 nm (60 °C), and 10 nm (80 °C). The colour scales represent a total height variation of 0.8 nm (20 °C, left), 0.15 nm (20°C, right), 0.1 nm (60 °C), and 0.5 nm (80 °C).

High-resolution imaging confirmed the broad range of interfacial assemblies, especially at temperatures above 50 °C. Representative images of the HOPG surface in Sq1:1Hd are shown in figure 10. At 20 °C the surface is relatively homogenous despite several aggregates present on the surface. Several row structures coexist with an inter-row spacing ranging between about 2.2 nm and 11.5 nm. Comparison with results in pure liquids (Fig. 4 and 6) suggests that both species are involved in the assembly. The structures are stable up to 40 °C, beyond which they tend to 'melt' leaving instead loosely epitaxial molecular structures with islands and grooves. Near surface features such of the HOPG such as atomic steps, the liquid appears to form large aggregates that can resist temperature beyond 80 °C. These aggregates act as anchoring points for the interfacial assemblies with rows and stable linear grooves appearing in their vicinity. No obvious molecular structure could be identified past 80 °C. In all cases and up to 100 °C, at least one layer remained on the HOPG surface which could not be imaged.

Squalane:Hexadecane 1:3 mixture

Shear force curves acquired in Sq1:3Hd exhibit a behaviour that combines features of Hd and Sq in their evolution with temperature and pressure (Fig. 11). The shear amplitude is

consistent with the evolution observed for Hd, showing an almost linear increase with tip force, relatively low values even at 20°C, and steady decrease with temperature. The phase, in contrast, exhibits the initial step at 0 nN followed by a plateau, consistent with results in Sq. The shear curves are remarkably reproducible between different locations of the sample, almost as in pure solvents. However, some variability could be seen between different cantilevers. Overall, these results suggest that at the interface with HOPG, Sq1:3Hd behaves as pure Hd in contact with an ordered Sq surface. The good stability of Sq at the surface of HOPG seems to induce preferential Sq adsorption although these results alone cannot exclude that this cohesive Sq-based layer also includes Hd molecules. Interestingly, the shear curves are relatively homogenous over the surface suggesting a reproducible molecular organisation at the interface. The shear phase exhibits a substantial elastic component comparable to that of pure Sq at 20 °C, but as the temperature increases the elastic behaviour is counter-intuitively reinforced. This could be explained by pinning of the tip in the Sq-based layer, the latter being weakened by the presence of Hd. This explanation is however speculative and experiments conducted with different tips showed some variations, although always with a significant elastic behaviour.

Overall, the shear results are supported by high-resolution imaging of the interface (Fig 12). At 20 °C a clear row structure is present in some area of the surface (2.1 nm spacing) suggesting that it is formed by Hd. The row structure is however not formed directly on the HOPG surface, but probably on a cohesive Sq layer, as confirmed by results at higher temperature. The rows are also fragile, unlike in pure Hd, further indication that they are on top of other molecular layer(s) assembled at the interface. Longitudinal islands are still visible at 30 °C with but tend to vanish past 40 °C often with disordered regions suggesting partial melting of the top layer. At 50 °C, different phase contrasts are visible across different regions of the surface (not shown), exactly as in pure Sq at 90°C (Fig. 4), indicating the existence of well-defined molecular layers on the HOPG surface, and with different molecular arrangements.

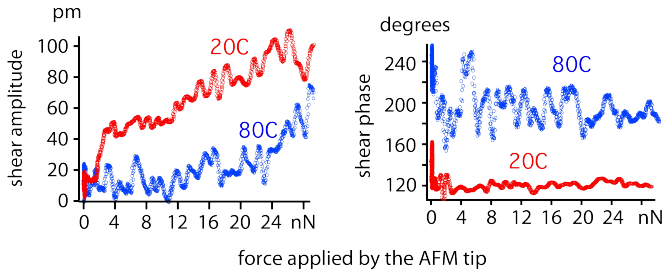

Fig 11 Representative curves of shear amplitude and corresponding phase as a function of the applied tip force at 20 °C and 80 °C. The shear amplitude exhibits an evolution similar to that in pure Hd (compare with Fig. 5 and S3), but the phase exhibits a step-increase at contact (0 nN), characteristic of measurements in pure Sq (Figs. 4 and S2). However, the phase values indicate a strong elastic component in the shear, amplified at 80 °C (taking into account a 180° offset compared to Fig. 3).

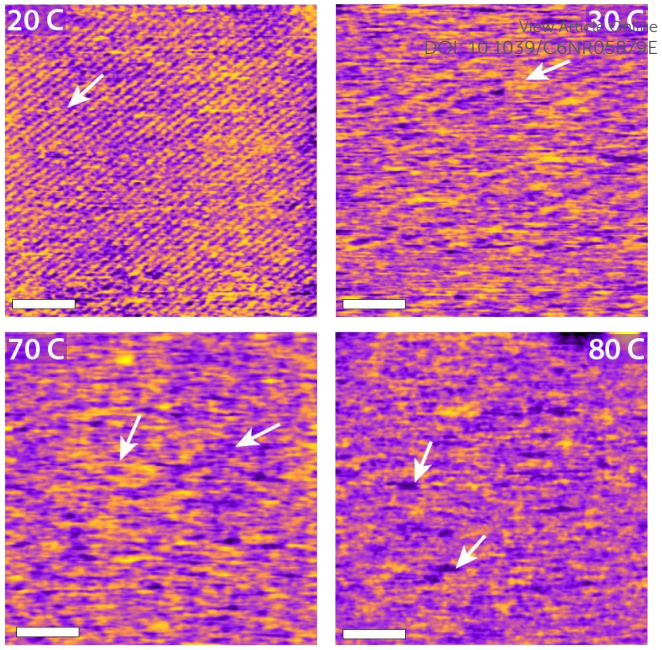

Fig 12 Selected high-resolution AFM images of HOPG in Sq1:3Hd at different temperatures. At 20 °C rows (spacing ~2.1 nm) are visible on the surface (arrow). The rows are fragile and easily removed by the tip already at 30 °C where they are hardly visible (arrow). At 70 °C, molecular islands are seen on the surface with hints of epitaxial effects suggesting an underlying hexagonal lattice (direction of the arrows). At 80 °C and higher, an unstructured layer remains on the surface, demonstrated by the presence of molecular point defects (arrows).

At higher temperatures, aggregates form near atomic steps of the HOPG (not shown) and epitaxial 'molecular islands' are visible on the surface. A stable layer is always present on the HOPG surface, suggesting it to be dominated by Sq.

General discussion

Pure liquids exhibit a continuous evolution with temperature when under confinement, but their behaviour completely depends on their molecular structure. Sq and Hd are both hydrophobic liquids that are composed of linear chains of carbon, and both show a strong affinity for HOPG with Hd achieving complete wetting[82]. The main difference resides in the side branching of Sq, which completely alters Sq interfacial behaviour under confinement. Previous work[81] has highlighted important differences between the two pure liquids under shear even without confinement. Not only the shape of the interface, but the molecular details of the liquids were shown to play a key role in the observed behaviour. Here, nanoscale imaging shows that Sq molecules create robust layers at the surface of HOPG that can resist temperatures beyond 100 °C under harsh shearing conditions (pressures in the order of 0.1 GPa). Studies of flat lying Sq monolayers on graphite have shown a melting temperature increased by > 90 °C compared to bulk Sq[83]. Present results show that contact of the interface with liquid Sq allows for more molecules to pack upright, hence creating strong inter-molecular interactions presumably due interlocking of the Sq side branches. This hinders molecular mobility and confer the adsorbed layers a solid-like behaviour. Shearing experiments support this view, with an

important elastic response of the confined layer that progressively decreases with increasing temperature but never completely disappears. Comparison with results in Hd3:1Sq suggests that the cohesive Sq monolayer effectively become the confining surface with limited contribution to the viscoelastic behaviour observed.

In contrast, Hd molecules are more mobile and the formation of self-assembled structures at the surface of HOPG can be easily undone by the scanning AFM tip, even using gentle imaging conditions. Above 90 °C, it was not possible to image the interface without completely displacing the molecules between the tip and the HOPG, occasionally revealing the atomic details of the HOPG surface. The shearing results in pure Hd suggest a largely viscous behaviour of the liquid at all temperatures, with the shear force decreasing as the temperature increases. The AFM results do not necessarily indicate that the interaction between HOPG and Hd molecules is weaker than between HOPG and Sq molecules. The more viscous behaviour of Hd comes from the absence of specific interactions between adjacent molecules, thus preventing the formation of a robust monolayer at all temperatures. The apparent strong affinity of the Sq monolayer for the HOPG surface can be explained by a group effect where a cohesive Sq patch binds to the HOPG.

Results obtained in liquid mixtures exhibit a rich variety of behaviours that can rarely be explained by a composition-weighted combination of the Sq and Hd behaviours. In the bulk, Hd and Sq appeared fully soluble at all the concentrations probed. However, when Sq molecules are present in the solution, they appear to dominate the behaviour of the confined liquid and replace Hd molecules at the surface of HOPG. This is hardly surprising given the robustness of the Sq layers under shear, compared to Hd. In Sq3:1Hd and Sq1:1Hd, the behaviour of the liquid under shear displays similar characteristics to pure Sq with an initial step change in amplitude and phase as the confining pressure increases. The final shear phase is however different, suggesting that the cohesive Sq layer can be altered by the presence of Hd, at least partially. In Sq1:3Hd, the behaviour is closer to that of pure Hd, but a stable molecular layer attributed to Sq is still present on the surface at all temperatures. This is not simply a case of higher affinity of Sq for the HOPG surface than Hd, but relates to more complex intermolecular interactions: despite HOPG being atomically flat, the shearing amplitudes and phases are found to often depend strongly on the location probed, suggesting the presence of different molecular arrangements at the interface, including possible clustering and nanoscale de-mixing of the solution. This variability is less marked for higher temperatures where viscous behaviour usually dominates both in Sq and Hd.

The dynamics of the liquid molecules in the layer immediately adjacent to the HOPG substrate depends on both liquid composition and temperature. High-resolution imaging and shear measurements indicate that the layer is solid-like at lower temperatures but can 'melt' at higher temperatures, as exemplified in Hd. A frozen layer typically allows reproducible imaging of molecular structures while the images become less clear upon partial or complete melting of the layer. This is due to the diffusion timescale of individual molecules becoming comparable to that of the AFM measurement. However, the fact that shear measurements always detect changes in amplitude and phase upon confinement indicate that the effective viscosity of this layer is higher than that of bulk liquid. It is well known that liquid molecules are often more ordered and less mobile at the interface with solids than in the bulk[34,35], in particular if they have some affinity for the solid. This interfacial effect dramatically influences the liquid's behaviour under confinement[27]. The results of this study highlight the fact that not only solid-liquid but also liquid-liquid molecular interactions determine the viscoelastic behaviour of the confined solution. Details of the shape, properties and organisation of the molecules at the interface are also crucial in understanding the shearing behaviour. Working with liquid mixtures adds considerable complexity to the system, especially if the interface can drive local de-mixing or clustering. The effect can become even more pronounced for interfaces where the confining solids present chemical and topological singularities such as roughness.

It should be noted that the experiment itself, in particular the nanoscale structure[84] and chemistry[85,86] of the tip, and the shearing speeds[11] are likely to play a role in the shearing observations but these aspects are not explored here, partly due to experimental constraints. Given the higher affinity of the liquids for the HOPG surface than the silicon oxide of the tip and the high curvature of the latter[87], it is reasonable to assume that the measurements are dominated by the interactions between the liquids and the HOPG surface. It was not possible to calculate the storage and loss moduli of the sheared liquid since the slip boundary conditions[26] are not known for each liquid nor their evolution with temperature. The shear amplitude and phase nonetheless provides a reliable and quantitative point of comparison between the different liquids studied.

Conclusions

This study examined the molecular organisation and behaviour of a dual paraffinic system under nano-confinement and at different temperatures using AFM. Shear experiments and high-resolution imaging of mixtures of Sq and Hd at the interface with atomically flat HOPG revealed a rich variety of behaviour that strongly depends on the local molecular organisation of the liquid. Pure Sq is viscoelastic under confinement at lower temperatures due to inter-molecular bonds that create cohesive interfacial layers. In contrast, pure Hd is largely viscous at all temperatures. Generally, the behaviour of mixtures is dominated by Sq, but it cannot be simply inferred from that of the pure components due to important local variations in the molecular arrangement at the nanoscale. As a result, measurements depend on the location probed despite the confining surfaces remaining identical. This variability diminishes at higher temperatures where Sq becomes more viscous.

Liquid mixtures often exhibit some nanostructure at interfaces due to differences in affinity between the surface and its component. Examples included monolayer, clusters or sponge-like molecular arrangements. This study highlights the importance of such structures in determining the behaviour of nano-confined liquids where molecular details take precedence over bulk properties.

Acknowledgements

This study was funded by BP Formulated Products Technology, which is gratefully acknowledged. Comments and proofreading by Mr. William Trewby is also acknowledged.

References

1 S. Gravelle, L. Joly, F. Detcheverry, C. Ybert, C. Cottin-Bizonne and L. Bocquet, *Proc. Natl. Acad. Sci. U. S. A.*, 2013, **110**, 16367–16372.
2 L. Bocquet and E. Charlaix, *Chem. Soc. Rev.*, 2010, **39**, 1073.
3 W. Sparreboom, A. van den Berg and J. C. T. Eijkel, *Nat. Nanotech.*, 2009, **4**, 713–720.
4 R. B. Schoch, J. Han and P. Renaud, *Rev. Mod. Phys.*, 2008, **80**, 839–883.
5 D. Chanda, K. Shigeta, S. Gupta, T. Cain, A. Carlson, A. Mihi, A. J. Baca, G. R. Bogart, P. Braun and J. A. Rogers, *Nat. Nanotech.*, 2011, **6**, 402–407.
6 C. Zhu, T. Y.-J. Han, E. B. Duoss, A. M. Golobic, J. D. Kuntz, C. M. Spadaccini and M. A. Worsley, *Nat. Commun.*, 2015, **6**, 6962.
7 D. Cohen-Tanugi and J. C. Grossman, *Nano Lett.*, 2012, **12**, 3602–3608.
8 U. F. Keyser, B. N. Koeleman, S. van Dorp, D. Krapf, R. M. M. Smeets, S. G. Lemay, N. H. Dekker and C. Dekker, *Nat. Phys.*, 2006, **2**, 473–477.
9 D. Branton, D. W. Deamer, A. Marziali, H. Bayley, S. A. Benner, T. Butler, M. Di Ventra, S. Garaj, A. Hibbs, X. Huang, S. B. Jovanovich, P. S. Krstic, S. Lindsay, X. S. Ling, C. H. Mastrangelo, A. Meller, J. S. Oliver, Y. V. Pershin, J. M. Ramsey, R. Riehn, G. V. Soni, V. Tabard-Cossa, M. Wanunu, M. Wiggin and J. A. Schloss, *Nat. Biotech.*, 2008, **26**, 1146–1153.
10 H. A. Stone, A. D. Stroock and A. Ajdari, *Annu. Rev. Fluid Mech.*, 2004, **36**, 381–411.
11 B. Bhushan, in *Fundamentals of Tribology and Bridging the Gap Between the Macro- and Micro/Nanoscales*, *2nd Ed.*, Springer Netherlands, Dordrecht, 2001, pp. 13–39.
12 B. Bhushan, J. Israelachvili and U. Landman, *Nature*, 1995, **374**, 607–616.
13 Y. Lei and Y. Leng, *Phys. Rev. Lett.*, 2011, **107**, 147801.
14 U. Tartaglino, B. N. J. Persson, A. I. Volokitin and E. Tosatti, *Phys. Rev. B*, 2002, **66**, 214207.
15 P. Nagendramma and S. Kaul, *Renew. Sustain. Energy Rev.*, 2012, **16**, 764–774.
16 L. Bocquet and J.-L. Barrat, *Soft Matter*, 2007, **3**, 685–693.
17 J. Williams, *Engineering Tribology*, Cambridge Univ. Press, Cambridge, 2015.
18 S. Granick, S. C. Bae, S. Kumar and C. Yu, *Physics*, 2010, **3**, 73.
19 J. Israelachvili, *Academic Press, London, 2nd Ed.*, 1992.
20 D. Gourdon and J. Israelachvili, *Phys. Rev. Lett.*, 2006, **96**, 099601.
21 J. Klein and E. Kumacheva, *Science*, 1995, **269**, 816–819.
22 C. Drummond and J. Israelachvili, *Phys. Rev. E*, 2001, **63**, 041506.
23 S. Granick, *Science*, 1991, **253**, 1374–1379.
24 Y. Zhu and S. Granick, *Phys. Rev. Lett.*, 2001, **87**, 096104.
25 S. H. Khan, G. Matei, S. Patil and P. M. Hoffmann, *Phys. Rev. Lett.*, 2010, **105**, 106101 EP –.
26 T.-D. Li and E. Riedo, *Phys. Rev. Lett.*, 2008, **100**, 106102.
27 D. Ortiz-Young, H. C. Chiu, S. Kim, K. Voitchovsky and E. Riedo, *Nat. Commun.*, 2013, **4**, 2482.
28 U. Raviv and J. Klein, *Science*, 2002, **297**, 1540–1543.
29 P. T. Cummings, H. Docherty, C. R. Iacovella and J. K. Singh, *AIChE J.*, 2010, **56**, 842–848.
30 T. Young, *Philo. Trans. Royal Soc. London*, 1804.
31 A. Dupré, *Théorie mécanique de la chaleur*, 1869.
32 K. Voïtchovsky, J. J. Kuna, S. A. Contera, E. Tosatti and F. Stellacci, *Nat. Nanotech.*, 2010, **5**, 401–405.
33 K. Voitchovsky and M. Ricci, Proc. SPIE, 2012, **8232**, 82320O.
34 W. Kaplan and Y. Kauffmann, *Annu. Rev. Mat. Res.*, 2006, **36**, 1–48.
35 C. Yu, G. Evmenenko, A. Richter, A. Datta, J. Kmetko and P. Dutta, *Appl. Surf. Sci.*, 2001, **182**, 231–235.
36 P. Fenter and N. Sturchio, *Prog. Surf. Sci.*, 2004, **77**, 171–258.
37 R. Lim and S. O'Shea, *Langmuir*, 2004, **20**, 4916–4919.
38 M. He, A. Szuchmacher Blum, G. Overney and R. E. Overney, *Phys. Rev. Lett.*, 2002, **88**, 154302.
39 S. Perkin, *Phys. Chem. Chem. Phys.*, 2012, **14**, 5052–5062.
40 S. O'Shea and M. Welland, *Langmuir*, 1998, **14**, 4186–4197.
41 J. Israelachvili, *Intermolecular and Surface Forces, 2nd Ed: With Applications to Colloidal and Biological Systems*, 1992.
42 S. de Beer, D. van den Ende and F. Mugele, *Nanotechnology*, 2010, 21, 325703.
43 R. Horn and J. Israelachvili, *J. Chem. Phys.*, 1981, **75**, 1400.
44 J. Sweeney, F. Hausen, R. Hayes, G. B. Webber, F. Endres, M. W. Rutland, R. Bennewitz and Rob Atkin, *Phys. Rev. Lett.*, 2012, **109**, 155502 EP –.
45 Y. Zhu and S. Granick, *Phys. Rev. Lett.*, 2004, **93**, 096101.
46 L. C. Zhang and K. Mylvaganam, *J. Comp. & Theo. Nano.*, 2006, **3**, 1–2.
47 E. Kumacheva, *Prog. Surf. Sci.*, 1998, **58**, 75–120.
48 C. I. Bouzigues, L. Bocquet, E. Charlaix, C. Cottin-Bizonne, B. Cross, L. Joly, A. Steinberger, C. Ybert and P. Tabeling, *Philo. Trans. Royal Soc.* 2008, **366**, 1455–1468.
49 M. Krasowska, M. N. Popescu and J. Ralston, *J. Phys.: Conf. Series*, 2012, **392**, 012009.
50 M. Broniatowski and P. Dynarowicz-Latka, *Wiad. Chem.*, 2004, **58**, 535–569.
51 S. Perkin, R. Goldberg, L. Chai, N. Kampf and J. Klein, *Faraday Discuss.*, 2009, **141**, 399–413.
52 R. Pashley and J. Israelachvili, *J. Coll. Interf. Sci.*, 1984, **97**, 446.
53 S. O'Shea, M. Welland and J. Pethica, *Chem. Phys. Lett.*, 1994, **223**, 336–340.
54 S. O'Shea, *Phys. Rev. Lett.*, 2006, **97**, 179601.
55 E. Riedo, *Membrane Tech.*, 2007, **2007**, 8–8.
56 S. Jeffery, P. M. Hoffmann, J. B. Pethica, C. Ramanujan, H. Ö. Özer and A. Oral, *Phys. Rev. B*, 2004, **70**, 054114.
57 S. H. Khan, E. L. Kramkowski, P. J. Ochs, D. M. Wilson and P. M. Hoffmann, *Appl. Phys. Lett.*, 2014, **104**, 023110.
58 T. Fukuma, Y. Ueda, S. Yoshioka and H. Asakawa, *Phys. Rev. Lett.*, 2010, **104**, 016101.

View Article Online
DOI: 10.1039/C6NR05879E

59 S. de Beer, D. Mannetje, S. Zantema and F. Mugele, *Langmuir*, 2010, **26**, 3280–3285.
60 G. Kaggwa, J. Kilpatrick, J. Sader and S. Jarvis, *Appl. Phys. Lett.*, 2008, **93**, 011909–011903.
61 L. Bureau, *Phys. Rev. Lett.*, 2010, **104**, 218302.
62 F. Liu, S. de Beer, D. van den Ende and F. Mugele, *Phys. Rev. E*, 2013, **87**, 062406.
63 R. Hayes, G. Warr and R. Atkin, *Phys. Chem. Chem. Phys.*, 2010, **12**, 1709–1723.
64 J. J. Segura, A. Elbourne, E. J. Wanless, G. G. Warr, K. Voitchovsky and R. Atkin, *Phys. Chem. Chem. Phys.*, 2013, **15**, 3320–3328.
65 J. Song, Q. Li, X. Wang, J. Li, S. Zhang, J. Kjems, F. Besenbacher and M. Dong, *Nat. Commun.*, 2014, **5**, 5837.
66 Q. Li, J. Song, F. Besenbacher and M. Dong, *Acc. Chem. Res.*, 2015, **48**, 119–127.
67 K. Voitchovsky, *Phys. Rev. E*, 2013, **88**, 022407.
68 T.-D. Li, J. Gao, R. Szoszkiewicz, U. Landman and E. Riedo, *Phys. Rev. B*, 2007, **75**, 115415.
69 J. L. Hutter and J. Bechhoefer, *Rev. Sci. Instrum.*, 1993, **64**, 1868–1873.
70 C. P. Green, H. Lioe, J. P. Cleveland, R. Proksch, P. Mulvaney and J. E. Sader, *Rev. Sci. Instrum.*, 2004, **75**, 1988–1996.
71 N. Mullin and J. K. Hobbs, *Rev. Sci. Instrum.*, 2014, **85**, 113703.
72 K. Voitchovsky, D. Giofrè, J. J. Segura, F. Stellacci and M. Ceriotti, *Nat. Commun.*, 2016, **7,** 13064.
73 M. Ricci, P. Spijker and K. Voitchovsky, *Nat. Commun.*, 2014, **5**, 4400.
74 E. J. Miller, W. Trewby, A. Farokh Payam, L. Piantanida, C. Cafolla and K. Voïchovsky, *J. Visual. Exp.*, 2016, **Accepted**.
75 W. Trewby, D. Livesey and K. Voitchovsky, *Soft Matter*, 2016, **12**, 2642–2651.
76 L. K. Thomas, A. Kühnle, S. Rode, U. Beginn and M. Reichling, *J Phys Chem C*, 2010, **114**, 18919–18924.
77 K. G. Nath, O. Ivasenko, J. M. MacLeod, J. A. Miwa, J. D. Wuest, A. Nanci, D. F. Perepichka and F. Rosei, *J. Phys. Chem. C*, 2007, **111**, 16996–17007.
78 L. P. Van, V. Kyrylyuk, J. Polesel-Maris, F. Thoyer, C. Lubin and J. Cousty, *Langmuir*, 2009, **25**, 639–642.
79 N. Gosvami, S. Sinha, W. Hofbauer and S. O'Shea, *J. Chem. Phys.*, 2007, **126**, 214708–214705.
80 N. Gosvami, S. Sinha and S. O'Shea, *Phys. Rev. Lett.*, 2008, **100**, 076101.
81 T. Schmatko, H. Hervet and L. Léger, *Phys. Rev. Lett.*, 2005, **94**, 244501.
82 I. C. Callaghan, D. H. Everett and A. J. P. Fletcher, *Faraday Trans. 1*, 1983, **79**, 2723.
83 A. D. Enevoldsen, F. Y. Hansen, A. Diama, L. Criswell and H. Taub, *J. Chem. Phys.*, 2007, **126**, 104703.
84 M. L. Bloo, H. Haitjema and W. O. Pril, *Measurement*, 1999, **25**, 203–211.
85 S. M. R. Akrami, H. Nakayachi, T. Watanabe-Nakayama, H. Asakawa and T. Fukuma, *Nanotechnology*, 2014, **25**, 455701.
86 K. Voitchovsky, *Nanotechnology*, 2015, **26**, 100501.
87 G. B. Kaggwa, P. C. Nalam, J. I. Kilpatrick, N. D. Spencer and S. P. Jarvis, *Langmuir*, 2012, **28**, 6589–6594.